COMMUNICATIONS IN COMPUTATIONAL PHYSICS
Vol. **1**, No. 3, pp. 528-547

Commun. Comput. Phys.
June 2006

A Nearly Analytical Discrete Method for Wave-Field Simulations in 2D Porous Media

Dinghui Yang[1,*], Jiming Peng[2], Ming Lu[1] and Tamas Terlaky[2]

[1] *Department of Mathematical Sciences, Tsinghua University, Beijing 100084, P. R. China.*
[2] *Department of Computing and Software, McMaster University, Hamilton, Canada.*

Received 5 September 2005; Accepted (in revised version) 11 January 2006

Abstract. The nearly analytic discrete method (NADM) is a perturbation method originally proposed by Yang *et al.* (2003) [26] for acoustic and elastic waves in elastic media. This method is based on a truncated Taylor series expansion and interpolation approximations and it can suppress effectively numerical dispersions caused by the discretizating the wave equations when too-coarse grids are used. In the present work, we apply the NADM to simulating acoustic and elastic wave propagations in 2D porous media. Our method enables wave propagation to be simulated in 2D porous isotropic and anisotropic media. Numerical experiments show that the error of the NADM for the porous case is less than those of the conventional finite-difference method (FDM) and the so-called Lax-Wendroff correction (LWC) schemes. The three-component seismic wave fields in the 2D porous isotropic medium are simulated and compared with those obtained by using the LWC method and exact solutions. Several characteristics of wave propagating in porous anisotropic media, computed by the NADM, are also reported in this study. Promising numerical results illustrate that the NADM provides a useful tool for large-scale porous problems and it can suppress effectively numerical dispersions.

Key words: Porous media; nearly-analytic discretization; three-component seismic wavefield; anisotropy; numerical dispersion.

1 Introduction

Usually, the oil/gas reservoir shows fractures, cracks, or pores, so it is a two-phase medium. On the basis of both the two-phase property of porous media and the analyses of the

*Correspondence to: Dinghui Yang, Department of Mathematical Sciences, Tsinghua University, Beijing 100084, P. R. China. Email: dhyang@math.tsinghua.edu.cn

 ©2006 Global-Science Press

solid/fluid interaction and coupling mechanisms, Biot established the theory of the elastic-wave propagation in a porous medium with saturated fluids for the low frequency [1] and the high frequency [2] cases, which is extraordinarily valuable for solving the problem of prospecting for oil and gas. Based on this theory, Biot predicted the slow P-wave that had been verified in the subsequent experiment [19]. To solve Biot's two-phase model and study the wave propagation in porous media with fluids, different numerical methods ([4, 6, 7, 13, 22, 23], others) have been proposed and studied.

Among various methods for seismic modeling in a porous medium, the finite-element method is one of most effective ones [23]. However, it requires expensive computational costs and large storage space compared with the finite-difference method (FDM), which prevents it from solving problems in higher dimension or large models. The FDM for modeling wave propagation is another popular tool due to its rapidity and lesser storage. Unfortunately, the conventional finite-difference methods with orders 2 and 4 often suffer from seriously numerical dispersion when too few samples per wavelength are used or when the models have large velocity contrast, or artifacts caused by source at grid points [9, 25]. Higher order FD (finite difference) methods such as high-order compact FD schemes also have numerical dispersions, and generally involve much more grid points when computing a displacement value at a grid-point (e.g. [5, 21]). Although numerical dispersions can also be suppressed via using a flux-corrected transport (FCT) technique [27], the FCT method can hardly recover the lost resolution by the numerical dispersion when the spatial sampling becomes too coarse [25]. On the other hand, acoustic and elastic waves have inherent dispersions as the waves propagate in a porous medium with fluids. This implies that two kinds of dispersions (numerical dispersion and wave dispersion) might appear simultaneously in wave fields if the conventional FD methods are used to compute the wave fields in a porous medium. In such a case, it is not a good idea to use the FCT technique to eliminate the numerical dispersions because we do not know how to choose the proper control parameters used in the FCT method for suppressing the numerical dispersions [25, 30]. The pseudo-spectral method [12, 15, 16] is attractive as the space operators are exact up to the Nyquist frequency. However, it requires the Fourier transform of the wave-field, which is computationally expensive for 3-D models and has difficulty in handing sharp boundaries [18]. The so-called nearly analytical discrete method (NADM), recently developed for solving acoustic and elastic equations [24, 26] and initially reported by Konddoh *et al.* (1994) [14] for solutions of parabolic and hyperbolic equations, can effectively eliminate the numerical dispersions without any additional treatments and has very high numerical accuracy. Moreover, compared with the conventional FD and finite-element methods for the single-phase case, the NADM requires less memory and is computationally cheaper [26].

Based on the above-mentioned points, in this paper we try to extend the NADM for the single-phase case to the two-phase case and present the robust NADM that is suitable for simulating acoustic and elastic waves propagating in 2D fluid-saturated porous media. Although the extension is not a difficult task, it is still far from being straightforward. To derive the NADM for the underlying problem, we first divide the order-two time derivatives

of coupling the solid and fluid displacements as presented in the Appendix A. Then, we convert the transformed wave equations into a system of first-order partial differential equations with respect to time. Finally, we design the NADM for the two-phase anisotropic case as that for the single-phase case [26].

2 Basic porous wave equations

Consider a 2D homogeneous porous medium. Acoustic and elastic waves propagating in the transversely isotropic (TI) porous medium can be described by the following equations [1] for the low frequency case:

$$\begin{aligned}
&\rho_{11}\begin{bmatrix}\ddot{u}_1^s\\ \ddot{u}_2^s\\ \ddot{u}_3^s\end{bmatrix}+\rho_{12}\begin{bmatrix}\ddot{u}_1^f\\ \ddot{u}_2^f\\ \ddot{u}_3^f\end{bmatrix}-\begin{bmatrix}b_{11}(\dot{u}_1^f-\dot{u}_1^f)\\ b_{11}(\dot{u}_2^f-\dot{u}_2^s)\\ b_{33}(\dot{u}_3^f-\dot{u}_3^s)\end{bmatrix}\\
=&\begin{bmatrix}
c_{11}\dfrac{\partial^2 u_1^s}{\partial x^2}+(c_{13}+c_{44})\dfrac{\partial^2 u_3^s}{\partial x\partial z}+c_{44}\dfrac{\partial^2 u_1^s}{\partial z^2}+Q_1\dfrac{\partial^2 u_1^f}{\partial x^2}+Q_1\dfrac{\partial^2 u_3^f}{\partial x\partial z}+F_1^s\\
c_{66}\dfrac{\partial^2 u_2^s}{\partial x^2}+c_{44}\dfrac{\partial^2 u_2^s}{\partial z^2}+F_2^s\\
c_{44}\dfrac{\partial^2 u_3^s}{\partial x^2}+(c_{13}+c_{44})\dfrac{\partial^2 u_1^s}{\partial x\partial z}+c_{33}\dfrac{\partial^2 u_3^s}{\partial z^2}+Q_3\dfrac{\partial^2 u_1^f}{\partial x\partial z}+Q_3\dfrac{\partial^2 u_3^f}{\partial z^2}+F_3^s
\end{bmatrix}, \qquad (2.1)\\
&\rho_{12}\begin{bmatrix}\ddot{u}_1^s\\ \ddot{u}_2^s\\ \ddot{u}_3^s\end{bmatrix}+\rho_{22}\begin{bmatrix}\ddot{u}_1^f\\ \ddot{u}_2^f\\ \ddot{u}_3^f\end{bmatrix}+\begin{bmatrix}b_{11}(\dot{u}_1^f-\dot{u}_1^s)\\ b_{11}(\dot{u}_2^f-\dot{u}_2^s)\\ b_{33}(\dot{u}_3^f-\dot{u}_3^s)\end{bmatrix}\\
=&\begin{bmatrix}
Q_1\dfrac{\partial^2 u_1^s}{\partial x^2}+Q_3\dfrac{\partial^2 u_3^s}{\partial x\partial z}+R(\dfrac{\partial^2 u_1^f}{\partial x^2}+\dfrac{\partial^2 u_3^f}{\partial x\partial z})+F_1^f\\
F_2^f\\
Q_1\dfrac{\partial^2 u_1^s}{\partial x\partial z}+Q_3\dfrac{\partial^2 u_3^s}{\partial z^2}+R(\dfrac{\partial^2 u_1^f}{\partial x\partial z}+\dfrac{\partial^2 u_3^f}{\partial z^2})+F_3^f
\end{bmatrix}, \qquad (2.2)
\end{aligned}$$

where $\ddot{u}_i^s=\partial^2 u_i^s/\partial t^2$, $\ddot{u}_i^f=\partial^2 u_i^f/\partial t^2$, $\dot{u}_i^s=\partial u_i^s/\partial t$, $\dot{u}_i^f=\partial u_i^f/\partial t$, $i=1,2,3$, $\rho_{11}=(1-\varphi)\rho_s+\rho_a$, $\rho_{22}=\varphi\rho_f+\rho_a$, and $\rho_{12}=-\rho_a$. $c_{11},c_{13},c_{33},c_{44},c_{66},Q_1,Q_3$, and R are the elastic constants of the porous medium. ρ_a is the additional density, and ρ_s and ρ_f are the densities of the solid and the fluid, respectively. b_{ii} $(i=1,3)$ are the dissipative coefficients determined by $\eta\varphi^2/k_{ii}$ with the viscosity η, the porosity φ, and the permeability k_{ii} in the i-direction. F_i^f and F_i^s are the total extraneous forces acting on the fluid and the solid in the i-direction, respectively. Specially, for the isotropic porous medium case we have $c_{13}=\lambda$, $c_{11}=c_{33}=\lambda+2\mu$, $c_{44}=c_{66}=\mu$, $Q_1=Q_3=Q$, $k_{11}=k_{33}$, and $b_{11}=b_{33}$. In other words, we can characterize the porous elasticity in terms of four elastic parameters λ, μ, Q, and R for the porous isotropic medium. Let

$$U=\left[u_1^f,u_2^f,u_3^f,u_1^s,u_2^s,u_3^s\right]^T,\ F=\left[F_1^f,F_2^f,F_3^f,F_1^s,F_2^s,F_3^s\right]^T,\ W=\dot{U},\ P=\ddot{U}.$$

Then we can rewrite (2.1) and (2.2) as (see Appendix A)

$$\frac{\partial^2}{\partial t^2}U = C_1\frac{\partial}{\partial t}U + C_2\frac{\partial^2}{\partial x^2}U + C_3\frac{\partial^2}{\partial x\partial z}U + C_4\frac{\partial^2}{\partial z^2}U + F = P. \tag{2.3}$$

For computational purposes, let us introduce the following vectors:

$$\overline{U} = \begin{bmatrix} U \\ \frac{\partial}{\partial x}U \\ \frac{\partial}{\partial z}U \end{bmatrix}, \quad \overline{P} = \begin{bmatrix} P \\ \frac{\partial}{\partial x}P \\ \frac{\partial}{\partial z}P \end{bmatrix}, \quad \overline{W} = \begin{bmatrix} W \\ \frac{\partial}{\partial x}W \\ \frac{\partial}{\partial z}W \end{bmatrix}. \tag{2.4}$$

It follows immediately that

$$\frac{\partial^{m+k+l+1}\overline{U}}{\partial t^{m+1}\partial x^k\partial z^l} = \frac{\partial^{m+k+l}\overline{W}}{\partial t^m\partial x^k\partial z^l} = \frac{\partial^{m+k+l-1}\overline{P}}{\partial t^{m-1}\partial x^k\partial z^l}, \tag{2.5}$$

where m, k, and l are nonnegative integers.

3 Nearly-analytic discrete method

On the basis of the above definitions, and using the values at the time t_n and the truncated Taylor series expansion, we obtain the following computational formulae, which similar to those of the NADM for the single-phase case [26]:

$$\overline{U}_{i,j}^{n+1} = \overline{U}_{i,j}^{n} + \Delta t\overline{W}_{i,j}^{n} + \frac{(\Delta t)^2}{2}\overline{P}_{i,j}^{n} + \frac{(\Delta t)^3}{6}\left(\frac{\partial\overline{P}}{\partial t}\right)_{i,j}^{n} + \frac{(\Delta t)^4}{24}\left(\frac{\partial^2\overline{P}}{\partial t^2}\right)_{i,j}^{n}, \tag{3.1}$$

$$\overline{W}_{i,j}^{n+1} = \overline{W}_{i,j}^{n} + \Delta t\overline{P}_{i,j}^{n} + \frac{(\Delta t)^2}{2}\left(\frac{\partial\overline{P}}{\partial t}\right)_{i,j}^{n} + \frac{(\Delta t)^3}{6}\left(\frac{\partial^2\overline{P}}{\partial t^2}\right)_{i,j}^{n}, \tag{3.2}$$

where Δt denotes the time increment. The expressions for$\overline{P}$, $\frac{\partial}{\partial t}\overline{P}$, and $\frac{\partial^2}{\partial t^2}\overline{P}$, which can be easily obtained using simple derivative operations, are listed in Appendix B.

Obviously, the more series terms $(\frac{\partial^k\overline{P}}{\partial t^k})_{i,j}^{n}(k = 0, 1, 2, \ldots)$ are kept in formulae (3.1) and (3.2), the more accurate the values of $\overline{U}_{i,j}^{n+1}$and $\overline{W}_{i,j}^{n+1}$ are. However, from a computational perspective, it is impossible to use the infinite Taylor series expansion. Instead, we refer to the truncated Taylor series expansions (3.1) and (3.2) that might lead to lower accuracy of $\overline{U}_{i,j}^{n+1}$and $\overline{W}_{i,j}^{n+1}$ because of the loss of wavefield information included in the higher-order terms in the Taylor series. To capture the lost wavefield information and further increase the computational accuracy, based on the "analysis thought" [14], we can approximately incorporate the lost information by using the connection relations and introducing the interpolation function. One way for this is to use implicit schemes that lead to costing storage because of the use of directly central-differencing the high-order time derivatives of $\overline{U}$ included implicitly in $(\frac{\partial^k\overline{P}}{\partial t^k})$ $(k = 1, 2)$ in (3.1) and (3.2). To avoid these problems, we propose converting these high-order time derivatives to the spatial derivatives

$(\frac{\partial^{k+l}U}{\partial x^k \partial z^l})^n_{i,j}$ $(2 \le k+l \le 5)$ for (3.1) and (3.2) and $(\frac{\partial^{k+l}\overline{W}}{\partial x^k \partial z^l})^n_{i,j}$ $(2 \le k+l \le 3)$ for equation (3.2). A similar conversion has been used in the high-order FD methods [5] and so-called Lax-Wendroff correction methods [3]. However, the way in which the NADM deals with the high-order spatial derivatives is significantly different from these used in high-order FD, Lax-Wendroff, and compact FD methods [17, 21]. The NADM is also different from the optimally accurate FDM developed by Geller and Takeuchi [10, 20], which uses a predictor-corrector scheme. The NADM introduces the following interpolation function, according to the Taylor series expansion on two variables,

$$G(X,Z) = \sum_{r=0}^{M} \frac{1}{r!}(X\frac{\partial}{\partial x} + Z\frac{\partial}{\partial z})^r U, \tag{3.3}$$

so that we determine these high-order spatial derivatives in terms of the following interpolation conditions between the grid point (i,j) and its eight neighboring nodes such as $(i-1,j)$, $(i+1,j)$, $(i,j-1)$, $(i,j+1)$, $(i-1,j-1)$, $(i-1,j+1)$, $(i+1,j-1)$, and $(i+1,j+1)$. For the case under our consideration, we choose $M=5$. Let us take the grid point $(i-1,j)$ as an example to illustrate these interpolation relations:

$$\begin{aligned} [G(-\Delta x,0)]^n_{i,j} &= U^n_{i-1,j}, \\ \left[\frac{\partial}{\partial X}G(-\Delta x,0)\right]^n_{i,j} &= (\frac{\partial}{\partial x}U)^n_{i-1,j}, \\ \left[\frac{\partial}{\partial Z}G(-\Delta x,0)\right]^n_{i,j} &= (\frac{\partial}{\partial z}U)^n_{i-1,j}. \end{aligned} \tag{3.4}$$

Here Δx is the spatial increment in the x-axis direction. Similarly, the other twenty-one connection relations at the nodes $(i-1,\, j+1)$, $(i-1,\, j-1)$, $(i,\, j+1)$, $(i,\, j-1)$, $(i+1,\, j+1)$, $(i+1,\, j)$, and $(i+1,\, j-1)$ can be easily written. According to these connection relations, we can obtain the analytic expressions of $\left(\frac{\partial^{k+l}U}{\partial x^k \partial z^l}\right)^n_{i,j}$ $(2 \le k+l \le 5)$ expressed by the displacement U and its gradient at the mesh point (i,j) and its neighboring grids (see Appendix C).

Note that, when computing $U^{n+1}_{i,j}$, the NADM uses not only the values of the displacement U at the mesh point $(i,\, j)$ and its neighboring grid points, but also the values of the partial derivatives of U with respect to time t and space x, z (see equations (3.1) and (3.2)). As a result, the NADM retains more wavefield information in both the function U^n and its first partial derivatives. Therefore, the NADM can effectively suppress the loss of information included in the higher-order terms of the Taylor expansion, resulting in great numerical accuracy and less numerical dispersions. The introduction of the local connection relations (3.4) improves greatly the continuity and derivability of the approximate function U^n (because U^n is an approximate variable during data processing) and furthermore stabilizes the NADM [26].

For the high-order derivatives of the so-called velocity $\overline{W}^n_{i,j}$ at the grid-point $(i,\, j)$ and time t_n, we can compute using the following backward difference method presented in the

previous study for the single-phase case [26]:

$$\left(\frac{\partial^{k+l}\overline{W}}{\partial x^k \partial z^l}\right)_{i,j}^{n} = \frac{1}{\Delta t}\left[\left(\frac{\partial^{k+l}\overline{U}}{\partial x^k \partial z^l}\right)_{i,j}^{n} - \left(\frac{\partial^{k+l}\overline{U}}{\partial x^k \partial z^l}\right)_{i,j}^{n-1}\right], \tag{3.5}$$

where $2 \leq k+l \leq 3$.

4 Error analysis

Using the Taylor series expansion, we find that the errors of $\frac{\partial^{m+l}U}{\partial x^m z^l}$ on $2 \leq m+l \leq 3$ and $4 \leq m+l \leq 5$) are $\mathcal{O}(\Delta x^4 + \Delta z^4)$ and $\mathcal{O}(\Delta x^2 + \Delta z^2)$, respectively, caused by the interpolation approximation. The error of $\frac{\partial^{m+l+1}U}{\partial t \partial x^m z^l}$ $(2 \leq m+l \leq 3)$ is $\mathcal{O}(\Delta t + \Delta x^4 + \Delta z^4)$, due to the use of the backward difference approximation (3.5) and the interpolation method. Therefore, the error introduced by the NADM is of the order of $\mathcal{O}(\Delta t^2 + \Delta x^4 + \Delta z^4)$ because of the use of equations (3.1) and (3.2) and the interpolation approximation, i.e. the NADM for the two-phase case is fourth-order accurate in space and second-order in time. This is the same as that for the single-phase case [26].

We take the acoustic wave equation in the 2D porous medium as an example to illustrate the accuracy of the NADM. In such a case, based on equation (2.3), the acoustic equation without the external force in a two-phase isotropic medium can be simplified to

$$\frac{\partial^2 u^s}{\partial t^2} = c_s^2\left(\frac{\partial^2 u^s}{\partial x^2} + \frac{\partial^2 u^s}{\partial z^2}\right), \tag{4.1a}$$

$$\frac{\partial^2 u^f}{\partial t^2} = c_f^2\left(\frac{\partial^2 u^s}{\partial x^2} + \frac{\partial^2 u^s}{\partial z^2}\right), \tag{4.1b}$$

where $c_f = \sqrt{\alpha\rho_{12}\mu}$ and $c_s = \sqrt{-\alpha\rho_{22}\mu}$. In order to investigate the numerical error of the NADM for the porous problem, we choose the following initial conditions:

$$u^s(0,x,z) = \cos[-2\pi f_0(x\cos\theta_0/c_s + z\sin\theta_0/c_s)], \tag{4.2a}$$

$$\frac{\partial u^s(0,x,z)}{\partial t} = -2\pi f_0 \sin[-2\pi f_0(x\cos\theta_0/c_s + z\sin\theta_0/c_s)], \tag{4.2b}$$

$$u^f(0,x,z) = \frac{c_f^2}{c_s^2}\cos[-2\pi f_0(x\cos\theta_0/c_s + z\sin\theta_0/c_s)], \tag{4.2c}$$

$$\frac{\partial u^f(0,x,z)}{\partial t} = -2\pi f_0 \frac{c_f^2}{c_s^2}\sin[-2\pi f_0(x\cos\theta_0/c_s + z\sin\theta_0/c_s)], \tag{4.2d}$$

where f_0 is the wave peak frequency and θ_0 is an incident angle at time $t = 0$.

Obviously, the analytical solution for the initial problem (4.1)-(4.2) is given by

$$u^s(t,x,z) = \cos\left[2\pi f_0(t - \frac{x}{c_s}\cos\theta_0 - \frac{z}{c_s}\sin\theta_0)\right],$$

$$u^f(t,x,z) = \frac{c_f^2}{c_s^2}\cos\left[2\pi f_0(t - \frac{x}{c_s}\cos\theta_0 - \frac{z}{c_s}\sin\theta_0)\right].$$

Table 1: Comparison of maximum $E_r(\%)$ for different cases and different methods.

Methods	Second-order FD	Fourth-order LWC	NADM
Case 1 : $h = 20m \quad \Delta t = 10^{-4}s$	50.542	0.7245	0.0682
Case 2 : $h = 40m \quad \Delta t = 5 \times 10^{-4}s$	179.961	11.862	0.6774
Case 3 : $h = 50m \quad \Delta t = 9 \times 10^{-4}s$	223.435	26.993	0.7481

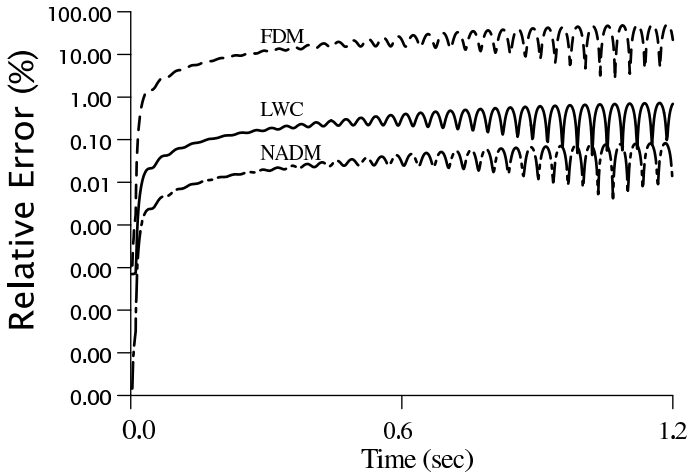

Figure 1: The relative errors of the second-order FDM ($- -$), LWC (—), and the NADM (— $-$) measured by E_r are shown in a semi-log scale for the 2-D initial problem (4.1)-(4.2). The spatial ($\Delta x = \Delta z$) and temporal increments are 20m and 10^{-4}s, respectively.

For comparison, we also use the second-order FDM and the so-called LWC (fourth-order compact scheme [5]) to solve the initial problem (4.1)-(4.2).

In our numerical experiments, the parameters are chosen as follows: the grid number $N = 150$, the frequency $f_0 = 15$Hz, the elastic constant $\mu = 4.38$ GPa, the solid-fluid coupling additional density $\rho_{12} = -0.42\text{g/cm}^3$, the solid density $\rho_s = 2.5\text{g/cm}^3$, the fluid density $\rho_f = 1.0\text{g/cm}^3$, the porosity $\varphi = 0.3$, and $\theta_0 = \pi/4$. The relative error (E_r) is the ratio of the RMS of the residual ($u^n_{i,j} - u(t_n, x_i, z_j)$) and the RMS of the exact solution $u(t_n, x_i, z_j)$. Its explicit definition is

$$E_r(\%) = 100 \times \left\{ \frac{\sum_{i,j=1}^{N} \left[u^n_{i,j} - u(t_n, x_i, z_j) \right]^2}{\sum_{i,j=1}^{N} \left[u(t_n, x_i, z_j) \right]^2} \right\}^{\frac{1}{2}}. \tag{4.3}$$

Figs. 1-3 show the computational results of the relative error E_r at different times for cases of different spatial and time increments, where three lines of E_r for the second-order FDM (line FDM), the fourth-order LWC (line LWC), and the NADM (line NADM)

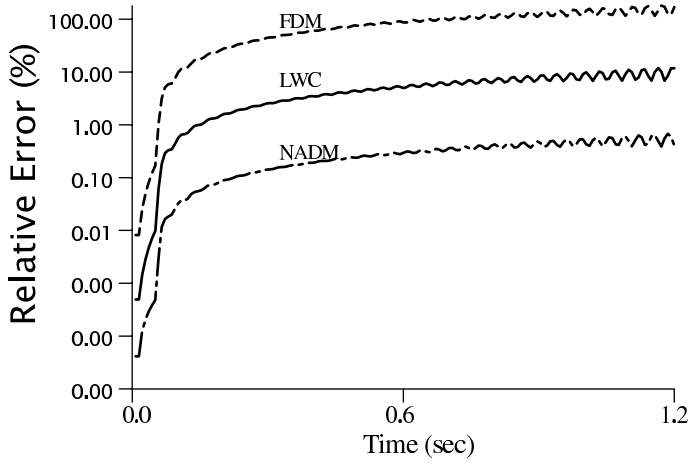

Figure 2: The relative errors of the second-order FDM ($--$), LWC (—), and the NADM (— $-$) measured by E_r are shown in a semi-log scale for the 2-D initial problem (4.1)-(4.2). The spatial ($\Delta x = \Delta z$) and temporal increments are 40m and 5×10^{-4}s, respectively.

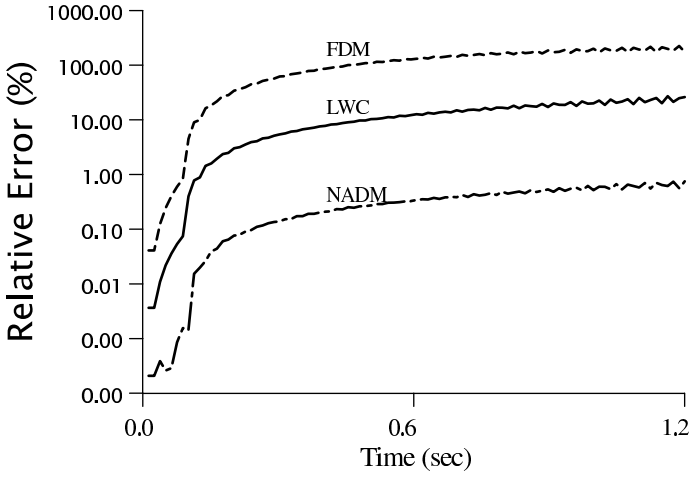

Figure 3: The relative errors of the second-order FDM ($--$), LWC (—), and the NADM (— $-$) measured by E_r are shown in a semi-log scale for the 2-D initial problem (4.1)-(4.2). The spatial ($\Delta x = \Delta z$) and temporal increments are 50m and 9×10^{-4}s, respectively.

are shown in a semi-log scale. From Figs. 1-3 we can conclude that the numerical error introduced by the NADM measured by E_r is less than those of the conventional FDM and the fourth-order LWC. In these figures, the maximum relative errors for different cases are listed in Table 1. From these error curves and Table 1 ($\Delta x = \Delta z = h$), we find that E_r increases corresponding to the increase in the time and/or spatial increments for all the three methods. As Figs. 1-3 illustrates, the NADM has the highest numerical accuracy among all three methods.

Table 2: Medium parameters used in Example 1.

λ (GPa)	μ (GPa)	Q (GPa)	R (GPa)	ρ_s g cm^{-3}	ρ_f g cm^{-3}	ρ_a g cm^{-3}	φ	b_{11}	b_{33}
7.24	4.38	1.14	0.331	2.5	1.0	0.42	0.3	225	225

5 Wave fields modeling

In this section, we investigate the efficiency of the NADM for the isotropic (Example 1) and transversely isotropic (TI) (Example 2) porous cases, and compare against the so-called LWC method [5] by wave-field modeling.

Example 1 To investigate the efficiency of the NADM for the fluid-saturated porous case and properties of elastic waves propagating in the two-phase medium with both the energy dissipation and the viscous phase boundary, we choose the medium constants listed in Table 2. The spatial and time increments are $\Delta x = \Delta z = 50m$ and $\Delta t = 2 \times 10^{-3}$sec, respectively. The computational domain is $0 \le x \le 10km$, $0 \le z \le 10km$ and the number of grid points is 201×201. The source is an explosive source that is at the center of the computational domain and has a Ricker wavelet with a peak frequency of $f_0 = 15$Hz. The time variation of the source function is $\sin(2\pi f_0 t)\exp(-4\pi^2 f_0^2 t^2/16)$ [29].

Fig. 4 shows the 3-component snapshots computed by the NADM, where Fig. 4(b) presents the wavefield snapshot of the u_2^s component at time $t = 2.5$s and Figs. 4(a) and 4(c) show wavefield snapshots of horizontal and vertical components (u_1^s and u_3^s) at time $t = 1.3$s. It can be easily verified from Fig. 4(b) that the wavefront of the u_2^s component snapshot (S-wave in 2D isotropic porous medium) is a cycle, and from Figs. 4(a) and 4(c) that the fast compressional wave (fast P-wave) and shear wave (S-wave) are simultaneously presented in wavefield snapshots of u_1^s and u_3^s component records. For the viscous phase boundary case, we can also observe the damping vibration (Figs. 4(a) and 4(c)) while we did not observe the slow P-wave in our experiment. This coincides with the strong attenuation of the slow P-wave, which means the slow P-wave can hardly be observed in practical seismic observations because real media are generally two-phase materials with viscous phase boundaries. Actually, in this case, the wave equation becomes a diffusion equation. Therefore, the slow P-wave propagation shows the diffusivity or heat conductivity and its attenuation is very high [28]. As interpreted by Geertsma and Smit (1961) [11], the third terms on the left-hand side of equations (2.1) and (2.2) are dominating and the solution of the poroelastic wave equation degenerates to that of a diffusion equation. The computations of generating the results in Fig. 4 were performed on a Pentium 4 with 256 MB memory, and it took about 34 minutes for generating wavefield snapshots of horizontal and vertical components (Figs. 4(a) and 4(c)), and about 20 minutes for generating Fig. 4(b).

To examine the validity of the NADM, we compare numerical results computed by the NADM and the so-called LWC method with 4-order accuracy. The snapshots of seismic

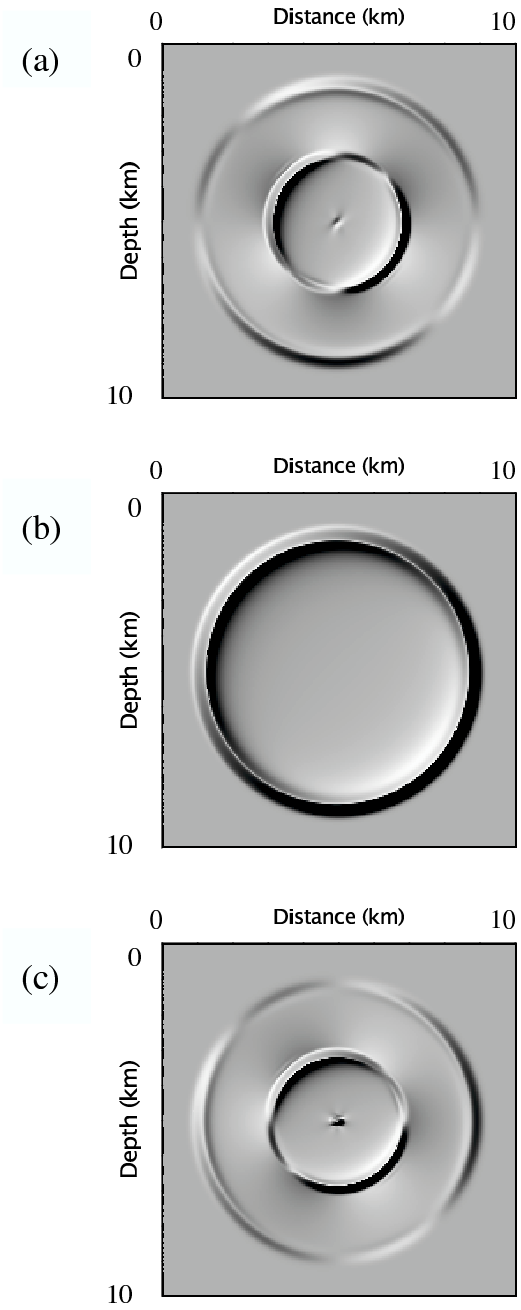

Figure 4: Snapshots of seismic wave fields for solid three-components in the porous isotropic medium (Example 1), generated by the NADM on the coarse-grid step, for (a) u_1^s component and (c) u_3^s component at time $t = 1.3$sec, and (b) u_2^s component at time $t = 2.5$sec.

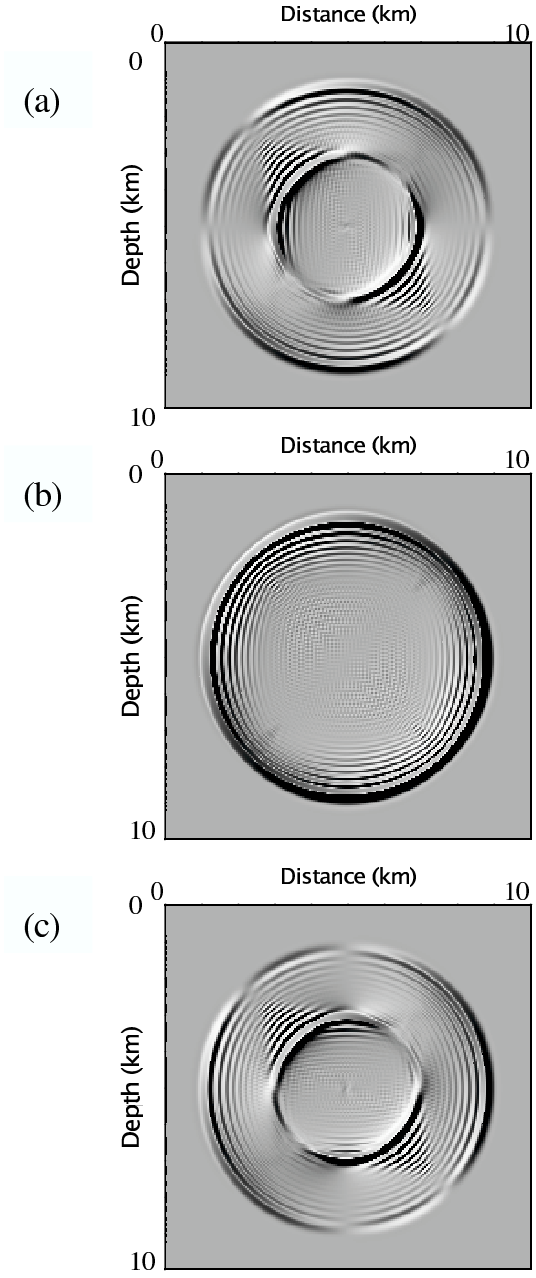

Figure 5: Snapshots of seismic wave fields for solid three-components in the porous isotropic medium (Example 1), generated by the LWC on the coarse-grid step, for (a) u_1^s component and (c) u_3^s component at time $t = 1.3$sec, and (b) u_2^s component at time $t = 2.5$sec.

Table 3: Medium parameters used in Example 2.

c_{11} (GPa)	c_{13} (GPa)	c_{33} (GPa)	c_{44} (GPa)	c_{66} (GPa)	Q_1 (GPa)	Q_3 (GPa)	R (GPa)	ρ_s g cm^{-3}	ρ_f g cm^{-3}	ρ_a g cm^{-3}	φ	b_{11}	b_{33}
26.4	6.11	15.6	4.8	9.6	1.14	0.95	0.331	2.34	1.0	0.083	0.108	225	350

wave-fields modeled by the LWC are presented in Fig. 5. We can see that the wavefronts of seismic waves simulated by two kinds of methods at the same time are basically identical (see Figs. 4 and 5). However, the snapshots in Fig. 5 simulated by the 4th-order LWC present strong numerical dispersion, and the corresponding results in Fig. 4 computed by the NADM show that the NADM has almost no numerical dispersion even if the space increment chosen is 50m without any additional treatments. It indicates that the NADM enables wave propagation to be simulated in large-scale porous models through using the coarse computation grids. Meanwhile, from Fig. 5 generated by the LWC we can see that the wavefront of the S-wave is slightly anisotropic. In other words, the velocity of the S-wave at different propagating directions is different. It shows that the LWC on the coarse grid can produce numerical anisotropy, initially noticed by Blanch and Robertsson (1997) [3].

To further test the efficiency of the NADM, the snapshot, computed by the 4th-order LWC on the fine-grid step ($\Delta x = \Delta z = 15m$ and $\Delta t = 6 \times 10^{-4}$sec) so that the grid dispersion caused by the LWC is eliminated, is shown in Fig. 6, whereas Fig. 4(b) is generated on the coarse-grid step ($\Delta x = \Delta z = 50m$ and $\Delta t = 2 \times 10^{-3}$sec) resulting in the same Courant number ($c_0\Delta t/\Delta x$, c_0 notes the sound velocity). Figs. 4(b) and 6 show that the NADM on a coarse grid can provide generally identical result to the LWC on a finer grid but with less memory and less computational cost. In other words, the NADM on a coarse grid can obtain generally identical exact solution as the high-order LWC converges [3, 5]. In our experiment, the NADM took about 20 minutes CPU time to generate Fig. 4(b), whereas the LWC used roughly 162 minutes to generate Fig. 6 under the same computing environment. The required storage for the LWC method is about 2.3 times of that for the NADM. When computing a value at a grid point, the NADM involves only 3 grid points in a direction while the 4th-order LWC needs 5 grid points [5]. The demand of more grid points in high-order LWC methods prevents the algorithms from efficient parallel implementation and artificial boundary treatment.

Example 2 In this example, we choose the transversely isotropic porous model with a vertical symmetry axis (TIV) and medium parameters listed in Table 3. The remaining computational parameters (e.g. coarse spatial and time increments, computational domain, frequency) and computer environment are the same as those in Example 1.

The wavefield snapshots of components for u_1^s, u_2^s, and u_3^s at time 1.3s are given in Fig. 7. We can see from Fig. 7(b) that the wavefront of quasi SH-wave (qSH) is an ellipse and the quasi P-(qP) and quasi SV-waves (qSV) (Figs. 7(a) and 7(c)) show the directional dependence on propagation velocities. The qSV wavefronts can have cusps and triplications depending on the value of C_{13} [8]. Triplications can be observed in the

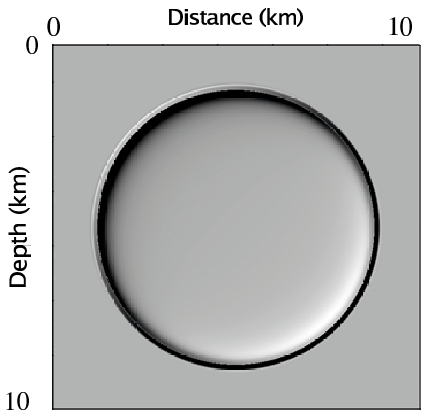

Figure 6: Snapshots of acoustic wave fields for solid u_2^s component at time $t = 2.5$sec in the porous isotropic medium (Example 1), generated by the LWC on a finer grid.

horizontal component qSV-wavefronts (shown in Fig. 7(a)) and in the vertical component qSV-wavefronts presented in Fig. 7(c). In addition, different arrival times for qP- and qS-waves and shear-wave splitting in the porous TIV medium can be seen from the wavefield snapshots shown in Fig. 7. On the same computer, it took the NADM about 34 minutes to generate Figs. 7(a) and 7(c) and about 13 minutes to generate Fig. 7(b).

6 Discussion and conclusions

The NADM for fluid-saturated porous media (including isotropic and anisotropic cases), which is similar to that for single-phase media [26], is developed via the Taylor series expansion and the interpolation approximate method, i.e., the time derivatives are approximated analytically by a truncated Taylor series and the space derivatives are calculated using the interpolation approximation. On the basis of such a structure, we have first to convert these high-order time derivatives to the spatial derivatives, which is similar to the high-order FD or so-called LWC methods [3, 5]. However, the NADM in approximating the high-order spatial derivatives is different from these high-order FD, LWC, and compact FD methods that use a discrete expression to approximate the original wave equation. The NADM uses simultaneously both the wave displacement and its gradients to approximate the high-order derivatives (see formulae (C.1-C.5)). When computing $U_{i,j}^{n+1}$, the NADM uses not only the values of the displacement U at the mesh point (i, j) and its neighboring grid points, but also the values of the displacement gradient and the so-called velocity $\overline{W}^n$. As a result, the NADM retains more wavefield information in both the function U^n and its gradients and the velocity $\overline{W}^n$. Therefore, the NADM can effectively suppress the loss of wavefield information included in the higher-order terms of the Taylor expansion, resulting in great numerical accuracy and less numerical dispersions. In fact, the numerical error of the NADM is less than those of the conventional 2-order FDM and 4-order LWC for the three models that we have presented. Wave-field modeling illustrates that

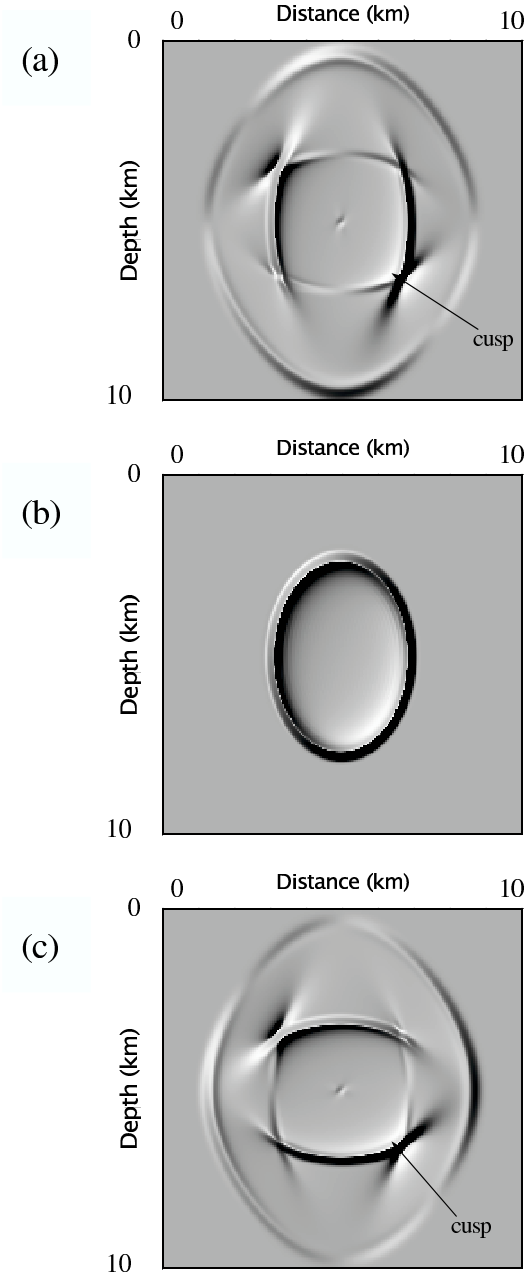

Figure 7: Snapshots of seismic wave fields for solid three-components at time $t = 1.3$sec in the porous TIV medium (Example 2), generated by the NADM on the coarse-grid step, for (a) u_1^s component, (b) u_2^s component, and (c) u_3^s component.

the NADM can effectively suppress numerical dispersions when too-coarse computation grids are used. These numerical results also illustrate that simultaneously using both the wave displacement and its gradients to approximate the high-order derivatives is important for decreasing the numerical dispersion caused by the discretization of wave equations because wave displacement gradients include important wavefield information. It suggests that we should consider the wave displacement gradient and velocity fields as we design a new numerical method to solve the porous acoustic and elastic wave equations.

We observe that if the same number of grid points is used, the CPU time of the NADM is more than that of the high-order LWC. However, since the NADM yields less numerical dispersion than the LWC with 4-order accuracy, we can increase the time increment through adopting coarser spatial increments to achieve the same accuracy as that of the LWC on a finer grid with smaller time steps. Hence, to achieve the same accuracy, the NADM takes less CPU than that of the LWC. As observed in our experiment, the computational speed of the NADM is 8 times faster than that of the 4th-order LWC on a finer grid. On the other hand, although the NADM involves additional gradient and velocity fields that require additional storage space, the required memory of the NADM based on coarse grids is only about 43% of storage space of the 4th-order LWC on a finer grid.

An interesting topic for future study is to consider the parallel computing for local difference operators in NADM to further improve its efficiency. It is also of interest to study the stability condition and test the algorithm in 3D media.

Appendix A: Wave equation transformations

Let the right sides of equations (2.1) and (2.2) equal to D and $\tilde{D}$, respectively, i.e.,

$$D=\begin{bmatrix} c_{11}\frac{\partial^2 u_1^s}{\partial x^2}+(c_{13}+c_{44})\frac{\partial^2 u_3^s}{\partial x\partial z}+c_{44}\frac{\partial^2 u_1^s}{\partial z^2}+Q_1\frac{\partial^2 u_1^f}{\partial x^2}+Q_1\frac{\partial^2 u_3^f}{\partial x\partial z}+F_1^s \\ c_{66}\frac{\partial^2 u_2^s}{\partial x^2}+c_{44}\frac{\partial^2 u_2^s}{\partial z^2}+F_2^s \\ c_{44}\frac{\partial^2 u_3^s}{\partial x^2}+(c_{13}+c_{44})\frac{\partial^2 u_1^s}{\partial x\partial z}+c_{33}\frac{\partial^2 u_3^s}{\partial z^2}+Q_3\frac{\partial^2 u_1^f}{\partial x\partial z}+Q_3\frac{\partial^2 u_3^f}{\partial z^2}+F_3^s \end{bmatrix},$$

$$\tilde{D}=\begin{bmatrix} Q_1\frac{\partial^2 u_1^s}{\partial x^2}+Q_3\frac{\partial^2 u_3^s}{\partial x\partial z}+R\frac{\partial^2 u_1^f}{\partial x^2}+R\frac{\partial^2 u_3^f}{\partial x\partial z}+F_1^f \\ F_2^f \\ Q_1\frac{\partial^2 u_1^s}{\partial x\partial z}+Q_3\frac{\partial^2 u_3^s}{\partial z^2}+R\frac{\partial^2 u_1^f}{\partial x\partial z}+R\frac{\partial^2 u_3^f}{\partial z^2}+F_3^f \end{bmatrix}.$$

Then we can rewrite equations (2.1) and (2.2) as

$$\rho_{11}\frac{\partial^2}{\partial t^2}U^s+\rho_{12}\frac{\partial^2}{\partial t^2}U^f-B\frac{\partial}{\partial t}(U^f-U^s)=D, \tag{A.1}$$

$$\rho_{12}\frac{\partial^2}{\partial t^2}U^s+\rho_{22}\frac{\partial^2}{\partial t^2}U^f+B\frac{\partial}{\partial t}(U^f-U^s)=\tilde{D}, \tag{A.2}$$

where $U^s=[u_1^s,u_2^s,u_3^s]^T$, $U^f=\left[u_1^f,u_2^f,u_3^f\right]^T$, and $B=\mathrm{diag}(\mathrm{b}_{11},\mathrm{b}_{11},\mathrm{b}_{33})$.

It follows from (A.1) and (A.2) that

$$\frac{\partial^2}{\partial t^2}U^f = \alpha\left[B(\rho_{12}+\rho_{11})\frac{\partial}{\partial t}(U^f-U^s)+\rho_{12}D-\rho_{11}\tilde{D}\right], \tag{A.3}$$

$$\frac{\partial^2}{\partial t^2}U^s = \alpha\left[-B(\rho_{12}+\rho_{22})\frac{\partial}{\partial t}(U^f-U^s)+\rho_{12}\tilde{D}-\rho_{22}D\right], \tag{A.4}$$

where $\alpha = 1/(\rho_{12}^2-\rho_{11}\rho_{22})$. Let

$$U = \left[u_1^f,u_2^f,u_3^f,u_1^s,u_2^s,u_3^s\right]^T, \quad F^s = [F_1^s,F_2^s,F_3^s]^T, \quad F^f = \left[F_1^f,F_2^f,F_3^f\right]^T.$$

Then we can rewrite (A.3) and (A.4) into the form

$$\frac{\partial^2}{\partial t^2}U = C_1\frac{\partial}{\partial t}U + C_2\frac{\partial^2}{\partial x^2}U + C_3\frac{\partial^2}{\partial x\partial z}U + C_4\frac{\partial^2}{\partial z^2}U + F, \tag{A.5}$$

where

$$F = \alpha\begin{bmatrix} \rho_{12}F^s-\rho_{11}F^f \\ \rho_{12}F^f-\rho_{22}F^s \end{bmatrix},$$

$$C_1 = \alpha\begin{bmatrix} (\rho_{12}+\rho_{11})B & -(\rho_{12}+\rho_{11})B \\ -(\rho_{12}+\rho_{22})B & (\rho_{12}+\rho_{22})B \end{bmatrix},$$

$$C_2 = \alpha\begin{bmatrix} \rho_{12}Q_1-\rho_{11}R & 0 & 0 & \rho_{12}c_{11}-\rho_{11}Q_1 & 0 & 0 \\ 0 & 0 & 0 & 0 & \rho_{12}c_{66} & 0 \\ 0 & 0 & 0 & 0 & 0 & \rho_{12}c_{44} \\ \rho_{12}R-\rho_{22}Q_1 & 0 & 0 & \rho_{12}Q_1-\rho_{22}c_{11} & 0 & 0 \\ 0 & 0 & 0 & 0 & -\rho_{22}c_{66} & 0 \\ 0 & 0 & 0 & 0 & 0 & -\rho_{22}c_{44} \end{bmatrix},$$

$$C_3 = \alpha\begin{bmatrix} 0 & 0 & \rho_{12}Q_1-\rho_{11}R & 0 & 0 & \rho_{12}c_{134}-\rho_{11}Q \\ 0 & 0 & 0 & 0 & 0 & 0 \\ \rho_{12}Q_3-\rho_{11}R & 0 & 0 & \rho_{12}c_{134}-\rho_{11}Q_3 & 0 & 0 \\ 0 & 0 & \rho_{12}R-\rho_{22}Q_1 & 0 & 0 & \rho_{12}Q_1-\rho_{22}c_{134} \\ 0 & 0 & 0 & 0 & 0 & 0 \\ \rho_{12}R-\rho_{22}Q_3 & 0 & 0 & \rho_{12}Q_3-\rho_{22}c_{134} & 0 & 0 \end{bmatrix},$$

$$C_4 = \alpha\begin{bmatrix} 0 & 0 & 0 & \rho_{12}c_{44} & 0 & 0 \\ 0 & 0 & 0 & 0 & \rho_{12}c_{44} & 0 \\ 0 & 0 & \rho_{12}Q_3-\rho_{11}R & 0 & 0 & \rho_{12}c_{33}-\rho_{11}Q_3 \\ 0 & 0 & 0 & -\rho_{22}c_{44} & 0 & 0 \\ 0 & 0 & 0 & 0 & -\rho_{22}c_{44} & 0 \\ 0 & 0 & \rho_{12}R-\rho_{22}Q_3 & 0 & 0 & \rho_{12}Q_3-\rho_{22}c_{33} \end{bmatrix}.$$

In the above definitions, $c_{134} = c_{13}+c_{44}$.

Appendix B: Computational expressions for $\overline{P}$, $\frac{\partial}{\partial t}\overline{P}$, and $\frac{\partial^2}{\partial t^2}\overline{P}$

Using the definition of the vector $\overline{P}$ (2.4), we have

$$\frac{\partial}{\partial t}\overline{P}=\left[\frac{\partial}{\partial t}P,\ \frac{\partial^2}{\partial t\partial x}P,\ \frac{\partial^2}{\partial t\partial z}P\right]^T,\quad \frac{\partial^2}{\partial t^2}\overline{P}=\left[\frac{\partial^2}{\partial t^2}P,\ \frac{\partial^3}{\partial t^2\partial x}P,\ \frac{\partial^3}{\partial t^2\partial z}P\right]^T,$$

where P is defined by (2.3), i.e.

$$P=C_1\frac{\partial}{\partial t}U+C_2\frac{\partial^2}{\partial x^2}U+C_3\frac{\partial^2}{\partial x\partial z}U+C_4\frac{\partial^2}{\partial z^2}U+F.$$

Direct calculations can represent the components of $\overline{P}_t$ and $\overline{P}_{tt}$ by U, W, F. For example,

$$\begin{aligned}
\frac{\partial}{\partial t}P&=C_1P+C_2\frac{\partial^2}{\partial x^2}W+C_3\frac{\partial^2}{\partial x\partial z}W+C_4\frac{\partial^2}{\partial z^2}W+\frac{\partial}{\partial t}F,\\
\frac{\partial}{\partial x}P&=C_1\frac{\partial}{\partial x}W+C_2\frac{\partial^3}{\partial x^3}U+C_3\frac{\partial^3}{\partial x^2\partial z}U+C_4\frac{\partial^3}{\partial x\partial z^2}U+\frac{\partial}{\partial x}F,\\
\frac{\partial^2}{\partial t^2}P&=C_1\frac{\partial}{\partial t}P+C_2\frac{\partial^2}{\partial x^2}P+C_3\frac{\partial^2}{\partial x\partial z}P+C_4\frac{\partial^2}{\partial z^2}P+\frac{\partial^2}{\partial t^2}F.
\end{aligned}$$

Similarly, we can easily obtain derivatives of $\frac{\partial^2 P}{\partial t\partial x}$, $\frac{\partial^2 P}{\partial t\partial z}$, $\frac{\partial^3 P}{\partial t^2\partial x}$, and $\frac{\partial^3 P}{\partial t^2\partial z}$.

Appendix C: Evaluation of the high-order partial derivatives of the displacement U

To apply the formula (3.1) to compute the values of U at time t_{n+1} in synthetic seismograms, we need to approximate some high-order derivatives. To this end, we have introduced the interpolation relations (3.4), following the "analysis thought" [14]. Using the interpolation relations such as equation (3.4) between the grid point $(i,\ j)$ and its eight neighboring nodes: $(i-1,\ j)$, $(i+1,\ j)$, $(i,\ j-1)$, $(i,\ j+1)$, $(i-1,\ j-1)$, $(i-1,\ j+1)$, $(i+1,\ j-1)$, and $(i+1,\ j+1)$, we can approximate the high-order partial derivatives of the displacement U at the grid-point $(i,\ j)$ as follows:

$$\partial_{2x}U^n_{i,j}=\frac{2}{\Delta x^2}\delta_x^2U^n_{i,j}-\frac{1}{2\Delta x}(E_x^1-E_x^{-1})\partial_xU^n_{i,j},\tag{C.1}$$

$$\partial_{2z}U^n_{i,j}=\frac{2}{\Delta z^2}\delta_z^2U^n_{i,j}-\frac{1}{2\Delta z}(E_z^1-E_z^{-1})\partial_zU^n_{i,j},\tag{C.2}$$

$$\begin{aligned}
\partial_{xz}U^n_{i,j}=&\frac{1}{2\Delta x}(E_x^1-E_x^{-1})\partial_zU^n_{i,j}+\frac{1}{2\Delta z}(E_z^1-E_z^{-1})\partial_xU^n_{i,j}\\
&-\frac{1}{4\Delta x\Delta z}(E_x^1E_z^1-E_x^1E_z^{-1}-E_x^{-1}E_z^1+E_x^{-1}E_z^{-1})U^n_{i,j},
\end{aligned}\tag{C.3}$$

$$\partial_{3x}U^n_{i,j}=\frac{15}{\Delta x^3}(E_x^1-E_x^{-1})U^n_{i,j}-\frac{3}{2\Delta x^2}(E_x^1+8I+E_x^{-1})\partial_xU^n_{i,j},\tag{C.4}$$

$$\partial_{3z}U^n_{i,j}=\frac{15}{\Delta z^3}(E_z^1-E_z^{-1})U^n_{i,j}-\frac{3}{2\Delta z^2}(E_z^1+8I+E_z^{-1})\partial_zU^n_{i,j},\tag{C.5}$$

where Δx and Δz are the spatial increments in the x- and z-axis directions, $U^n_{i,j}$, $\partial_x U^n_{i,j}$, $\partial_z U^n_{i,j}$, and $\partial_{mxkz} U^n_{i,j}$ denote $U(i\Delta x, j\Delta z, n\Delta t)$, $\frac{\partial}{\partial x}U(i\Delta x, j\Delta z, n\Delta t)$, $\frac{\partial}{\partial z}U(i\Delta x, j\Delta z, n\Delta t)$, and $\left(\partial^{m+k}U/\partial x^m \partial z^k\right)^n_{i,j}$, respectively. Moreover, the notations δ_z^2 and E_z in equations (C.1)-(C.5) are the second central difference and displacement operators in the z-direction, respectively, namely

$$\delta_z^2 U^n_{i,j} = U^n_{i,j+1} - 2U^n_{i,j} + U^n_{i,j-1}, \quad E_z^1 U^n_{i,j} = U^n_{i,j+1}, \quad E_z^{-1} U^n_{i,j} = U^n_{i,j-1}$$

The operators δ_x^2 and E_x in the x-direction can be similarly written. Other computational formulae are omitted here.

Most formulas and notations above are essentially the same as those used in the original NADM [26]. The difference is that the displacement is defined by $U = [u_x, u_z, u_y]^T$ in NADM [26] and by $U = [u_1^f, u_2^f, u_3^f, u_1^s, u_2^s, u_3^s]^T$ in our present work.

Acknowledgments

We thank Dr. Enru Liu for his valuable comments that greatly improved the manuscript. This work was supported by the National Natural Sciences Foundation of China (Grant 40574014) and the MCME of China. Part of this work was done when the first author visited the Department of Computing and Software, McMaster University. The visit was partially supported by the MITACS project "New interior point methods and software for convex conic linear optimization with applications to solving VLSI circuit layout problems". The research of the second author was partially supported by the grant #RPG 249635-02 of the National Sciences and Engineering Research Council of Canada (NSERC), a PREA award from Ontario, and the above-mentioned MITACS project.

References

[1] M. A. Biot, Theory of propagation of elastic waves in a fluid-saturated porous solid, I. Low-frequency range, J. Acoust. Soc. Am., 28 (1956), 168-178.
[2] M. A. Biot, Theory of propagation of elastic waves in a fluid-saturated porous solid, II. Higher-frequency range, J. Acoust. Soc. Am., 28 (1956), 179-191.
[3] J. O. Blanch and J. O. A. Robertsson, A modified Lax-Wendroff correction for wave propagation in media described by Zener elements, Geophys. J. Int., 131 (1997), 381-386.
[4] J. M. Carcione, Wave simulation in anisotropic, saturated porous media, 65th Ann. Internat. Mtg., Soc. of Expl. Geophys., Expanded Abstracts, (1995), 1309-1312.
[5] M. A. Dablain, The application of high-order differencing to the scalar wave equation, Geophysics, 51 (1986), 54-66.
[6] N. Dai, A. Vafidis and E. R. Kanasewich, Wave propagation in heterogeneous, porous media: A velocity-stress, finite-difference method, Geophysics, 60 (1995), 327-340.
[7] V. Easwaran, W. Lauriks and J. P. Coyette, Displacement-based finite element method for guided wave propagation problems: Application to poroelastic media, J. Acoust. Soc. Am., 100 (1996), 2989-3002.

[8] E. L. Faria and P. L. Stoffa, Finite-difference modelling in transversely isotropic media, Geophysics, 59 (1994), 282-289.
[9] T. Fei and K. Larner, Elimination of numerical dispersion in finite-difference modeling and migration by flux-corrected transport, Geophysics, 60 (1995), 1830-1842.
[10] R. J. Geller and N. Takeuchi, Optimally accurate second-order time-domain finite difference scheme for the elastic equation of motion: one-dimensional case, Geophys. J. Int., 135 (1998), 48-62.
[11] J. Geertsma and D. C. Smit, Some aspects of elastic wave propagation in fluid saturated porous solids, Geophysics, 26 (1961), 169-181.
[12] B. S. Huang, A program for two-dimensional seismic wave propagation by the pseudospectrum method, Comput. Geosci., 18 (1992), 289-307.
[13] D. Komatitsch and J. P. Vilotte, The Spectral Element method: an efficient tool to simulate the seismic response of 2D and 3D geological structures, Bull. Seismol. Soc. Am., 88 (1998), 368-392.
[14] Y. Konddoh, Y. Hosaka and K. Ishii, Kernel optimum nearly analytical discretization algorithm applied to parabolic and hyperbolic equations, Comput. Math. Appl., 27 (1994), 59-90.
[15] D. Kosloff and E. Baysal, Forward modeling by a Fourier method, Geophysics, 47 (1982), 1402-1412.
[16] D. Kosloff, M. Reshef and D. Loewenthal, Elastic wave calculations by the Fourier method, Bull. Seismol. Soc. Am., 74 (1984), 875-891.
[17] S. K. Lele, Compact finite difference schemes with spectral-like resolution, J. Comput. Phys., 103 (1992), 16-42.
[18] H. Mizutani, R. J. Geller and N. Takeuchi, Comparison of accuracy and efficiency of time-domain schemes for calculating synthetic seismograms, Phys. Earth Planet In., 119 (2000), 75-97.
[19] T. J. Plona, Observation of a second bulk compressional wave in a porous medium at ultrasonic frequencies, Appl. Phys. Lett., 36 (1980), 259-261.
[20] N. Takeuchi and R. J. Geller, Optimally accurate second order time-domain finite difference scheme for computing synthetic seismograms in 2-D and 3-D media, Phys. Earth Planet In., 119 (2000), 99-131.
[21] S. Q. Wang, D. H. Yang and K. D. Yang, Compact finite difference scheme for elastic equations, J. Tsinghua Univ. (Sci. & Tech.), 42 (2002), 1128-1131, (in Chinese).
[22] W. J. Xu and J. Guo, Numerical simulation of elastic waves in fluid-Satuated porous media, Chinese J. Geophys-Ch, 37(Supp.1) (1994): 424-433.
[23] D. H. Yang, Finite element method of the elastic wave equation and wave-fields simulation in two-phase anisotropic media, Chinese J. Geophys-Ch., 45 (2002), 575-583.
[24] D. H. Yang, M. Lu, R. S. Wu and J. M. Peng, An optimal nearly-analytic discrete method for 2D acoustic and elastic wave equations, Bull. Seismol. Soc. Am., 94 (2004), 1982-1991.
[25] D. H. Yang, E. Liu, Z. J. Zhang and J. Teng, Finite-difference modelling in two-dimensional anisotropic media using a flux-corrected transport technique, Geophys. J. Int., 148 (2002), 320-328.
[26] D. H. Yang, J. W. Teng, Z. J. Zhang and E. Liu, A nearly-analytic discrete method for acoustic and elastic wave equations in anisotropic media, Bull. Seismol. Soc. Am., 93 (2003), 882-890.
[27] K. D. Yang, D. H. Yang and S. Q. Wang, Wave-field simulation based on the Biot-Squirt equation, Chinese J. Geophys-Ch., 45 (2002), 853-861.

[28] D. H. Yang and Z. J. Zhang, Poroelastic wave equation including the Biot/Squirt mechanism and the solid/fluid coupling anisotropy, Wave Motion, 35(3) (2002), 223-245.
[29] J. Zahradnik, P. Moczo and T. Hron, Testing four elastic finite-difference schemes for behavior at discontinuities, Bull. Seismol. Soc. Am., 83 (1993), 107-129.
[30] Z. J. Zhang, G. J. Wang and J. M. Harris, Multi-component wave-field simulation in viscous extensively dilatancy anisotropic media, Phys. Earth Planet In., 114 (1999), 25-38.